EFFECT OF GRAIN SIZE ON THE VAPOUR PHASE HYDRATION OF MONOCLINIC AND TRICLINIC MODIFICATIONS OF TRICALCIUM SILICATE; ROLE OF HIGH TEMPERATURE ACTIVATION

S. HANAFI[a], G. M. S. EL-SHAFEI[a] and B. ABD EL-HAMID[b]

[a] *Chemistry Department, Faculty of Science, Ain Shams University, Cairo, Egypt*
[b] *Physics Department, Faculty of Science, Ain Shams University, Cairo, Egypt*

Received November 2, 1990
Accepted April 10, 1991

The hydration of tricalcium silicate (C_3S) with three grain sizes of monoclinic (M) and triclinic (T) modifications and on their thermally activated samples were investigated by exposure to water vapour at 80°C for 60 days. The products were investigated by XRD, TG and N_2 adsorption. The smaller the particle size the greater was the hydration for both dried and activated samples from (M). In the activated samples a hydrate with 2θ values of 38·4°, 44·6° and 48·6° could be identified. Hydration increased with particle size for the unactivated (T) samples but after activation the intermediate size exhibited enhanced hydration. Thermal treatment at 950°C of (T) samples increased the surface active centers on the expense of those in the bulk. Changes produced in surface texture upon activation and/or hydration are discussed.

The interaction of tricalcium silicate (C_3S) with water has been extensively investigated in the paste or suspension form[1-7]. Under these conditions the various hydration stages greatly overlap in virtue of the high concentration of the water molecules. The attack of water onto C_3S from the vapour phase was studied by Fierens and others[8-10] who employed thermoluminescence technique in their study and showed the importance of the nucleophilic excited centers in the hydration process that form the initial chemisorptive bond in the C_3S–H_2O system.

Activation by thermal treatment[9] is found to modify both the characteristics of these active centers and the probability of escape of trapped electrons that have a marked influence on the rate of water chemisorption. Also the presence of lattice defects[11] in the grains was found to be directly related to the enhanced reactivity towards hydration.

In a previous study on the hydration of alite (C_3S) from the vapour phase[12], it has been shown that the penetration of water molecules into the lattice structure, after adsorption, causes the distortion of the cell dimensions giving rise to a pattern that bares some resemblance to the C_3S pseudo-cell structure prior to its chemical interaction with the solid matrix. Some investigators[13,14] employed a specific grain

size or area in their investigations but the problem to what extent does the grain dimension affect the different hydration stages was hardly attempted. The effect of polymorphism of C_3S on the initial hydration rate was also studied[5] in the paste form, where they noticed apparent differences in the morphology of the calcium silicate hydrate formed on the surface of the grain.

In this investigation the role of both grain size and polymorphism on the water vapour adsorption at 80°C was monitored using thermal, structural and textural techniques.

EXPERIMENTAL

Materials

Two crystalline modifications of C_3S were used, namely the monoclinic (MC_3S) and triclinic (TC_3S) forms supplied by Portland Cement Association (PCA) U.S.A. Three different grain sizes were employed, two of them possessed a Blain area of approx. 3 500 cm^2/g and approx. 2 200 cm^2/g and the third was an 8-mesh sample. The subscripts 1, 2 and 3 denote these three samples.

The particle size was analysed on a Sedigraph particle size analyzer using Sediperse A-12 as dispersant and carried out by Micrometrics (Fig. 1).

The free lime content determined in duplicate of the monoclinic and triclinic modifications gave an average of 0·7 and 0·4, respectively. The bulk chemical composition supplied by the PCA is given below in wt. %.

Modification	SiO_2	Al_2O_3	Fe_2O_3	CaO	MgO	K_2O	Na_2O	TiO_2
Monoclinic	26·75	0·94	0·09	72·95	0·50	0·01	0·03	0·45
Triclinic	27·05	0·91	0·06	73·70	0·28	0·01	0·02	0·16

Full scan X-ray pattern from 2° to 90° 2θ showed no secondary minerals to be present.

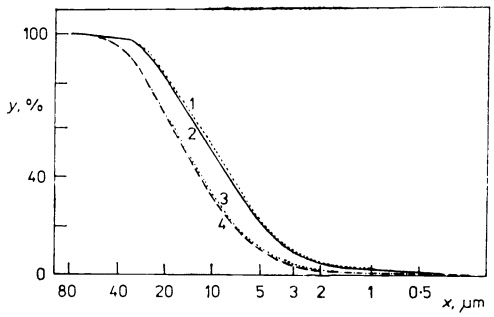

FIG. 1

Particle size distribution of samples: **1** $(TC_3S)_1$, 3 525 cm^2/g; **2** $(MC_3S)_1$, 3 525 cm^2/g; **3** $(TC_3S)_2$, 1 986 cm^2/g; **4** $(MC_3S)_2$, 1 965 cm^2/g; y cumulative weight percent, x equivalent spherical diameter

Thermal Treatment

All samples were dried at 120°C overnight and activation was achieved by heating at 950°C for two hours in air. The temperature of 950°C was found not to affect the structure of C_3S samples under investigation, being below the first transition temperature at 1 050°C (ref.[9]). As the rate of cooling usually affects the populaion of defects in the solid structure, it was controlled in the three grain sizes. After heating the samples at 950°C they were left to cool in the muffle furnace till the temperature reached 500°C, taking about 2 h and then placed in a desiccator (silica gel was used as dehydrating agent). The treatment temperature will be given in parenthesis when necessary.

Hydration of the Samples

The dried and activated samples were hydrated in the vapour phase at a temperature of 80°C (H_2O vapour pressure 47·343 kPa) (arbitrarily chosen to be below the b.p. of water). The samples were exposed to water vapour (free from any absorbed gases) at this temperature for 2 months — the experimental details are given elsewhere[12]. It is worth noting that no distillation of water to the samples took place during this period.

Apparatus and Technique

Thermogravimetric analyses of the samples were carried out using a Stanton–Redcroft thermobalance type 750/770 connected to a Kipp and Zonnen BD-9 two channel automatic recorder. The analyses were done in static air at a heating rate of 10 K/min.

The XRD patterns of the various hydration products were obtained using a Philips X-ray diffractometer, model PW 1140/90 using Ni-filtered Cu-radiation. The *d* distances were calculated and their relative intensities were compared with data in the ASTM cards[15,16].

Adsorption–desorption isotherms of purified N_2 were determined at −196°C using a conventional volumetric apparatus.

RESULTS AND DISCUSSION

Effect of Particle Size

Thermal and structural characteristics. Thermogravimetric analysis of the monoclinic and triclinic C_3S samples dried at 120°C showed no weight loss in the range ambient temperature − 1 000°C. They all exhibit the main characteristic X-ray bands of C_3S.

The TG curves of the monoclinic and triclinic samples hydrated at 80°C exhibit three main distinct regions of enhanced weight loss that characterize the decomposition of the resulting hydration products (Fig. 2, curves a, b, respectively). These regions are arbitrarily confined in the temperature ranges below 450°C, 450 − 750°C and above 750°C to indicate the first, second and final major decomposition stages. These result from physically adsorbed water, hydration water (which may as well have been dissociatively adsorbed to form hydroxyls) and decarbonation resulting from the carbonate produced by interaction with atmospheric CO_2. The percentage loss corresponding to each stage is given in Table I for all the samples.

To measure the extent of hydration, the first decomposition stage should be omitted being concerned with physically adsorbed water only. It appears more reasonable to take into account the intermediate and final decomposition stages to represent the extent of chemical interaction with water vapour, and not the total weight loss. These two stages are believed to represent together the products of reaction with water and can be employed as an alternative to the "non-evaporable" water estimated by some authors to evaluate the extent of reaction[17]. Accordingly, the extent of interaction for the various particle sizes is in the decreasing order of $(MC_3S)_1 > (MC_3S)_2 > (MC_3S)_3$.

From XRD analysis of the samples before and after hydration, the sample $(MC_3S)_3$ (largest grain size) is found to exhibit an increase in intensity for some of the smaller bands situated at 2θ values of 30·7, 31·54, 36·30, 45·20, 54·00 and 59·00° with a corresponding marked decrease in the characteristic bands for C_3S (Fig. 3). These bands are not identified as belonging to any well established hydration product of C_3S. In case of the other two grain sizes, a marked decrease in band intensity is observed with the disappearance of some of the bands whose intensity increased in the sample $(MC_3S)_3$. Simultaneously with this decrease in band intensity for the sample $(MC_3S)_1$, some weak bands for $Ca(OH)_2$ appear which clearly represent

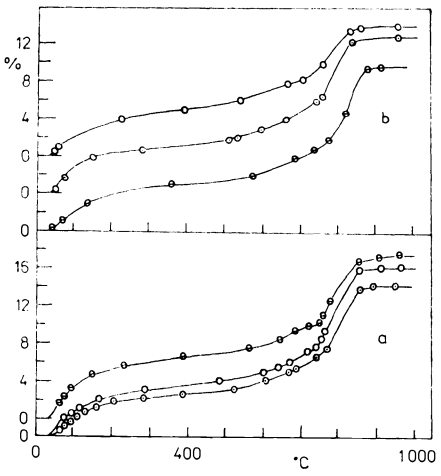

FIG. 2

Thermogravimetric curves for a monoclinic b triclinic C_3S samples dried at 120°C and hydrated at 80°C for 60 days ○$(C_3S)_1$; ◎$(C_3S)_2$; ⊖$(C_3S)_3$ weight loss in percent

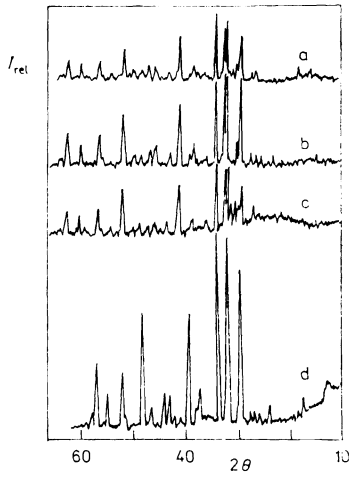

FIG. 3

X-Ray diffraction patterns for monoclinic C_3S samples dried at 120°C; a sample $(MC_3S)_2$ before hydration; b—d samples $(MC_3S)_1$, $(MC_3S)_2$ and $(MC_3S)_3$, respectively after hydration at 80°C

an advanced hydration stage. Combining these observations with the TG results it seems reasonable to believe that in the sample $(MC_3S)_2$, $Ca(OH)_2$ may also be present but in an amorphous state[18] or in very small crystallite dimensions (<5 nm).

Thus the initial hydration process partly destroys the crystalline pattern of monoclinic C_3S with the appearance of an intermediate, probably a metastable hydrate[6], characterized by the bands observed for the sample $(MC_3S)_3$. $Ca(OH)_2$ starts to form at a later stage in minute size (existing in an amorphous state), with the disappearance of this metastable hydrate as in the sample $(MC_3S)_2$. This amorphous $Ca(OH)_2$ gradually takes on its geometric shape at a further stage as found with the sample $(MC_3S)_1$. Comparable observations on large single crystals were also reported[7]. Thus the smaller particle $(MC_3S)_1$ is found to enhance hydration in the monoclinic modification.

TABLE I

Loss in weight of the three major decomposition stages obtained from TG analysis for the unhydrated and hydrated C_3S polymorphs

Sample	Initial loss <450°C %	Intermediate loss 450°–750°C %	Final loss >750°C %	Total loss %
		Before hydration		
$(TC_3S)_1(950)$	1·80	0·25	0·25	2·30
$(TC_3S)_2(950)$	2·45	0·50	0·45	3·40
$(TC_3S)_3(950)$	zero	0·35	1·05	1·40
		After hydration		
$(MC_3S)_1(120)$	6·00	12·40	8·00	18·40
$(MC_3S)_2(120)$	5·00	11·70	7·70	16·70
$(MC_3S)_3(120)$	6·90	10·95	7·20	17·80
$(TC_3S)_1(120)$	5·55	2·95	6·00	14·40
$(TC_3S)_2(120)$	5·60	4·20	7·40	17·20
$(TC_3S)_3(120)$	5·40	4·30	8·20	17·90
$(MC_3S)_1(950)$	6·00	13·80	8·00	19·80
$(MC_3S)_2(950)$	6·60	12·60	8·00	19·20
$(MC_3S)_3(950)$	7·40	9·30	5·10	16·70
$(TC_3S)_1(950)$	4·65	2·75	6·60	14·00
$(TC_3S)_2(950)$	6·50	5·30	10·30	22·10
$(TC_3S)_3(950)$	4·40	2·35	5·95	12·60

When C_3S is in the triclinic form, the largest grain size shows an advanced hydration stage over the other two grain sizes; the sample $(TC_3S)_1$ exhibits a more retarded stage than $(TC_3S)_2$ (Table I, columns 3 and 4). In these samples a more significant parameter other than particle dimension is becoming active in the hydration process. The presence of available active centers at the surface and consequently their number seem to have a major role in this process[8,11]. From TG analysis (Fig. 2, curve b) no steps are observed at 400–550°C indicating the absence of free $Ca(OH)_2$ which was also not found in the X-ray patterns of the hydrated samples (Fig. 4). However, an increased weight loss is subsequently observed up to approx. 750°C that seems to result from the hydrate (or hydrates) formed, followed by a distinct step in the temperature range 800–850°C depending on particle size, that results from the decomposition of the carbonate.

Hydration of the C_3S triclinic samples results in a decrease in the X-ray bands characterizing C_3S with an increase in the band intensity of those at 2θ values of 30·82° and 31·65° being marked in the sample $(TC_3S)_1$ and analogous to those observed with the monoclinic modification, together with bands characterizing the presence of carbonate (calcite). In these samples no definite crystalline hydrate could be detected and the above mentioned bands appear to result from an ill-crystalline hydration product. However they are much reduced in the sample $(TC_3S)_3$ that also shows the highest percentage loss in the two intermediate stages of weight losses (Table I, columns 3 and 4). Thus when C_3S is in the triclinic modification its activity towards hydration increases with grain size.

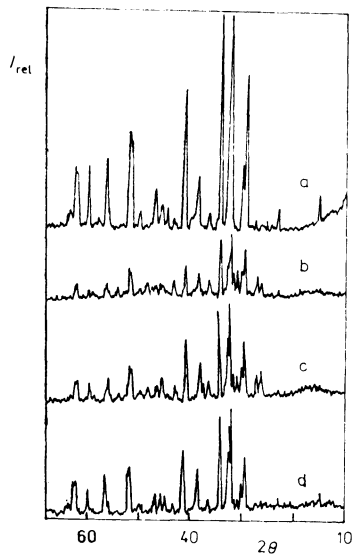

FIG. 4

X-Ray diffraction patterns for triclinic C_3S samples dried at 120°C: a sample $(TC_3S)_2$ before hydration, b–d samples $(TC_3S)_1$, $(TC_3S)_2$ and $(TC_3S)_3$, respectively after hydration at 80°C

Surface and pore characterization. Adsorption-desorption isotherms of N_2 at 77°K were obtained for the three grain sizes of the dried monoclinic and triclinic modifications before and after hydration. The isotherms are all on the border between Type II and Type III being characterized by a low BET *C*-constant. Before hydration, closed hysteresis loops are observed for the two smaller grain sizes from the monoclinic modification that disappeared upon hydration, whereas for the triclinic form, only the smallest grain size exhibited a small narrow hysteresis loop and after hydration all grain sizes showed small narrow hysteresis loops.

Though the early region of the isotherms do not show a well defined knee, yet the BET equation could be applied in its normal range of applicability to estimate the specific surface area (S_{BET}) assuming a value of 0·162 nm^2 as a cross-sectional area for the N_2 molecule. As all samples whose area is estimated by the BET equation exhibit low *C* constant, any error arising from the absence of a pronounced knee in the adsorption isotherms may be considered almost constant for all samples and consequently comparison of these specific areas would be meaningful.

Hydration of these monoclinic samples brings about an increase in specific surface area that is largest for the sample $(MC_3S)_1$, that was shown before to undergo enhanced hydration over the other two grain sizes (Table II, column 3). This increase in surface area is accompanied by a decrease in both total pore volume $V_{p(0.95)}$ and average pore radius ($\bar{r}_H$), (columns 5 and 6, resp.).

These changes are also reproduced through the pore structure analysis carried out according to the *t*-method of de Boer and coworkers[19]. The *t*-curve originally given by Mikhail et al.[20] characterized by a low BET *C*-constant is corrected for differences in the frequencies of oscillations of molecules or ions[21] of the adsorbent and reference solid as given by Selim et al.[22] to allow for a correct estimate of S_t (specific area obtained from V_l–*t* plot). The agreement between S_t and S_{BET} is clearly observed as shown in Table II (columns 4 and 3, respectively).

The V_l–*t* plots of the monoclinic C_3S modification show that before hydration, the sample $(MC_3S)_1$ exhibits an upward deviation in slope permitting capillary condensation to occur with multimolecular adsorption (Fig. 5, I). At very low *t*-values of 0·2–0·3 nm some points are negatively deviated that result from the presence of few micro pores and the sample is thus predominantly meso porous. For the other two grain sizes, $(MC_3S)_2$ and $(MC_3S)_3$, the upward deviation does not continue but soon reverts back to cut the straight line passing through the origin at *t*-values of 1·10 and 0·98 nm, respectively pointing to the increased microporosity that increases with grain size. The V_l–*t* plot of sample $(MC_3S)_3$ clearly shows that it possesses the narrowest pore dimension and is mainly composed of supermicro pores[23].

Hydration of these samples is accompanied by narrowing of the pore system; this is pronounced for the sample $(MC_3S)_1$ (Fig. 5, I), and sample $(MC_3S)_3$ is least affected. It seems that in this specific grain size of the sample, $(MC_3S)_1$ (smallest

size) either exposes the largest number of crystal defects which act as the initial nuclei[24] for the hydration process or that this particular size causes the exposure

TABLE II

Surface characteristics of monoclinic and triclinic C_3S samples dried at 120°C and their corresponding hydrated samples

Sample	BET *C*-constant	S_{BET} m^2/g	S_t m^2/g	$V_{p(0.95)}$ ml/g	$\bar{r}_H$ nm
		Before hydration			
$(MC_3S)_1(120)$	4·0	69·2	65·0	0·1498	2·16
$(MC_3S)_2(120)$	4·0	70·3	67·5	0·0889	1·26
$(MC_3S)_3(120)$	3·0	65·9	59·0	0·0714	1·03
$(TC_3S)_1(120)$	3·5	67·2	66·0	0·0840	1·25
$(TC_3S)_2(120)$	3·0	81·4	78·0	0·0850	1·05
$(TC_3S)_3(120)$	3·0	58·7	59·0	0·0640	1·05
		After hydration			
$(MC_3S)_1(120)$	3·0	76·6	77·0	0·1076	1·40
$(MC_3S)_2(120)$	3·0	72·5	67·0	0·0800	1·10
$(MC_3S)_3(120)$	3·0	67·0	60·5	0·0679	1·01
$(TC_3S)_1(120)$	3·5	56·5	53·9	0·0619	1·10
$(TC_3S)_2(120)$	4·0	65·1	62·0	0·0679	1·08
$(TC_3S)_3(120)$	3·0	60·7	56·5	0·0643	1·06

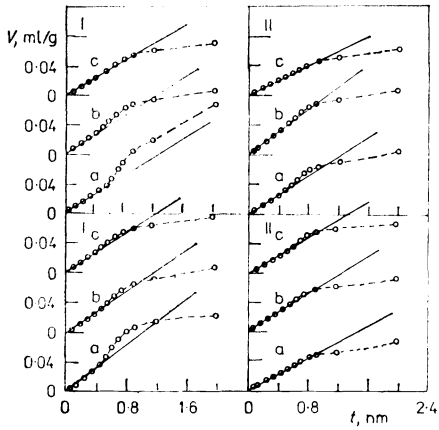

FIG. 5

V_l–t plots for monoclinic (I) and triclinic (II) C_3S samples dried at 120°C before and after hydration at 80°C for 60 days: a $(C_3S)_1$; b $(C_3S)_2$; c $(C_3S)_3$

of certain planes, as found with some oxide systems[25] which have preferential adsorption of water vapour. This adsorbed water may at first be bound by physical forces then gradually undergoes a chemical reaction[11] probably after penetration into the lattice if not originally chemisorbed on the surface.

In the triclinic modification, the sample $(TC_3S)_2$ possesses the highest area and the smallest average pore radius among the series (Table II, column 3). Hydration of the samples is accompanied by a decrease in specific surface area for the two samples of smaller grain sizes whereas the area is almost unaffected for sample $(TC_3S)_3$. From the previous observations it follows that the 8-mesh sample contained more hydration products than the other two grain sizes. If the initial stages of hydration are accompanied by a decrease in area, the increased amounts of hydration products in the sample should at a certain stage contribute to the increase in area. The initial hydration stages may possess pores that are inaccessible to the N_2 molecules. The total pore volume slightly decreased for the two smaller grain sizes, whereas the average pore radius is almost unaffected for all the samples.

The V_l–t plots of the triclinic C_3S samples show all the three grain sizes to be composed of a mixture of micro and meso pores in which the latter are in the low size range (Fig. 5, II). The V_l–t plot of sample $(TC_3S)_1$ shows clearly the occurrence of some capillary condensation to take place thus reflecting the existence of some wider pores as compared to the other two samples of larger grain size. The changes induced in the pore system upon hydration are negligible except for the sample $(TC_3S)_1$ where some narrowing of the pores is observed that is also reflected in the data of the average pore radius (Table II, column 6).

Effect of Activation at 950°C

Thermal and structural changes. The monoclinic C_3S samples activated at 950°C showed no weight loss in the range ambient temperature 1 000°C whereas the triclinic modification is more affected by this activation being reflected in the corresponding TG curves of the three grain sizes (Fig. 6, curve a). No other component than C_3S could be detected in the XRD patterns of the activated samples. However, from IR spectral analysis for both modifications, bands at 3 400 cm^{-1} and 1 600 cm^{-1} arising from the stretching and bending modes of the O—H vibrational frequency of adsorbed water appeared as well as a band in the frequency range 1 400 to 1 500 cm^{-1} characterising the presence of a carbonate $(CaCO_3)$[26]. It is interesting to note that the TG of the sample $(TC_3S)_3(950)$ of largest grain size, does not exhibit any weight loss below 420°C where all the adsorbed water appears to undergo chemical interaction with the solid (1·4% total loss). These observations were absent for samples dried at 120°C. Thus activation at 950°C seems to increase the active centers at the surface in localized parts[24] that readily adsorb water vapour from the atmosphere and initiate the hydration process to proceed. At these active centers,

the $Ca(OH)_2$ formed as a hydration products further interacts with the atmospheric CO_2 to form the carbonate. If the intermediate and final stages of percentage losses of TC_3S are taken into consideration, the largest grain size is found to be the most sensitive towards atmospheric H_2O and CO_2 (Table I, columns 3 and 4).

The hydration at 80°C of these samples is also enhanced only for the two smaller grain sizes as seen from both polymorphs compared to that of the hydrated dried samples; the largest grain size show retarded hydration (Table I) for both forms.

In case of monoclinic C_3S, the hydration increases with decrease of particle size as previously observed for the dried samples, however that the largest grain size heated at 950°C gives lower hydration products than the corresponding sample heated at 120°C is quite peculiar. Likewise in the triclinic modification, though the largest grain size of the hydrated dried sample shows the maximum hydration products, the corresponding sample heated at 950°C exhibits the least reaction inspite that it was most reactive upon exposure to atmospheric H_2O and CO_2. It thus seems reasonable to believe that there should be some active centers in the solid matrix to aid in the continuity of the reaction. When these migrate to the surface by heat treatment at 950°C they induce excess activity to the surface at the expense of the bulk activity thus giving the observed effects in the largest grain size. It is significant to note that samples showing maximum loss in the intermediate stage (Table I, column 3) are those that show enhanced activity.

From the TG curves of the monoclinic samples it is noted that the sample $(MC_3S)_1$. .(950), that actually represents the most advanced reacted hydration stage, shows a clear step at approx. 500°C representing the decomposition of $Ca(OH)_2$ (Fig. 6, b).

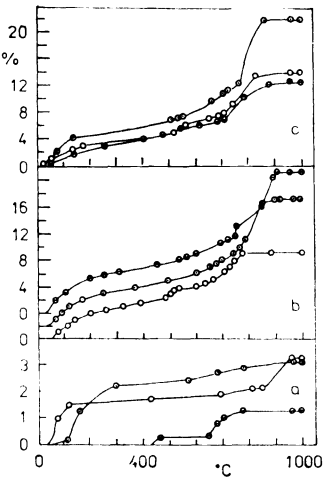

FIG. 6

Thermogravimetric curves for samples activated at 950°C: a Triclinic C_3S before hydration; b monoclinic C_3S after hydration; c triclinic C_3S hydration weight loss in %

Its presence is clearly observed in the XRD patterns where the bands are well defined and their intensities are found to decrease with increase in particle size (Fig. 7). Some bands for vaterite (μ-$CaCO_3$) are also observed. Though all hydrated samples show reduced bands of the crystalline pattern of C_3S yet some new bands of relatively strong intensities appear with *d* distances of 327·5, 275·5, 234·4, 206·6, 203·0 and 187·3 pm. Not all of these appear in the samples $(MC_3S)_2$ and $(MC_3S)_3$ but are much reduced for the latter both in number and intensity with the appearance of two small peaks at 2θ range of $30·7-32·0°$ that also appeared with the hydrated dried samples. No tobermorite-like structure could be detected. It is important to note that three of the main new bands characterizing the hydrate formed and clearly identified in the sample $(MC_3S)_1(950)$ are according to their decreasing intensities at 2θ values of $38·4° > 44·6° > 48·6°$ (*d* distances of 234·4, 203·0 and 187·3 pm) do not characterize together any known hydration product of C_3S (ref.[27]). The 187·3 pm band actually constitutes one of the strong bands for a C_3S hydrate[28] but some other strong bands at 328 or 289 pm should have appeared as well with a nearly equivalent intensity which is not the case. The band appearing at $2\theta = 27·2°$ has a much lower intensity than required for this reported C_3S hydrate as well as it does not include a band at 234·4 pm. We thus believe that this pattern may either represent a new phase of C_3S hydrate alone or mixed with some undefined C_2S hydrate.

From the above observations on the effect of activation temperature on the hydration reaction, the samples can be put in the increasing hydration order of $(MC_3S)_3(120) < (MC_3S)_2(120) \simeq (MC_3S)_3(950) < (MC_3S)_1(120) < (MC_3S)_2(950) < <(MC_3S)_1(950)$.

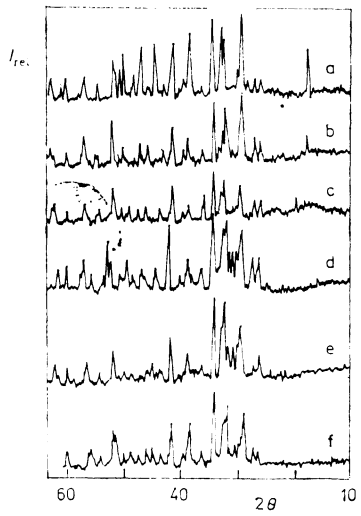

FIG. 7

X-Ray diffraction patterns for samples activated at 950°C and hydrated at 80°C for 60 days: a—c samples $(MC_3S)_1$, $(MC_3S)_2$ and $(MC_3S)_3$, respectively; d—f samples $(TC_3S)_1$, $(TC_3S)_2$ and $(TC_3S)_3$, respectively

In case of the triclinic C_3S samples, activation at 950°C enhanced the hydration of the sample with intermediate size, $(TC_3S)_2$, but not of the other two grain sizes where the hydration is almost unaltered for the sample of smallest grain size and decreased for the largest grain size compared to the hydration of the dried samples (Table I).

The TG curve of sample $(TC_3S)_3$ is characterized by two steps in the intermediate stage at approx. 500°C and 535°C besides that in the final stage at 750°C (Fig. 6, curve c). From XRD data, only two hydration products could be identified, a tobermorite gel and $CaCO_3$, then the step at 500°C probably results from amorphous $Ca(OH)_2$. Also bands at 2θ of 38·35° and 44·60° (d distance of 236 and 202 pm, respectively), that are close to those observed for the hydrated sample $(MC_3S)_1(950)$, are intensified for the sample $(TC_3S)_3(950)$ only (Fig. 7). This raises the belief that the small step observed in the TG curve at 535°C results from a hydration product which is responsible for increasing the intensity of these bands that are destroyed upon further hydration. They may represent the initial stages of formation of the hydration product in the tobermorite gel. The sample $(TC_3S)_3(950)$ represents a more retarded hydration stage as compared to the samples $(TC_3S)_2(950)$ or $(TC_3S)_1(950)$ and the order of increased hydration may be put as $(TC_3S)_3 < < (TC_3S)_1 < (TC_3S)_2$.

Variations in the textural characteristics. The N_2 adsorption–desorption isotherms of the activated samples from both modifications are also between Type II and Type III and are still characterized by a low BET C-constant except that of the sample $(MC_3S)_2(950)$ and the hydrated sample $(MC_3S)_3(950)$ that are Type III (BET C-constant < 3). For both modifications and with all grain sizes the isotherms exhibit closed hysteresis loops of variable sizes. Hydration of the samples causes a marked narrowing of these loops and completely disappearing for the sample $(TC_3S)_1(950)$.

Specific surface areas evaluated for samples from the monoclinic form show that activation causes a small increase in area for the sample $(MC_3S)_1$, whereas a decrease is observed for the sample $(MC_3S)_2$ while the sample $(MC_3S)_3$ (8-mesh) seems to be unaffected (Tables II and III, column 3). The presence of relatively more carbonate in the sample $(MC_3S)_1(950)$ than in other grain sizes as detected by IR spectroscopy (not presented here) seems to be responsible for this small increase in area. The samples characterized by BET C-constant < 3 had their areas evaluated for comparison only by assuming an approximate value for the constant C and locating[29] $(P/P_0)_m$ from which the monolayer capacity can be obtained, but are still considered unreliable.

The changes in specific area observed for the samples $(MC_3S)_2$ and $(MC_3S)_3$ (compared to the dried samples) are accompanied by an increase in both total pore volume $V_{p(0.95)}$ and average pore radius $\bar{r}_H$ (Table III, columns 5 and 6). Such effects result from the agglomeration of the particles upon heating. It is significant

to recall that the bulk chemical nature of these samples is unaltered upon activation at 950°C (except for the surface active centers that seem to have reacted with the atmosphere after activation).

These results are reflected in the V_l–t plots of the samples $(MC_3S)_1$ and $(MC_3S)_3$ (Fig. 8, l). The small upward deviation at 0·48 nm of the sample $(MC_3S)_1(950)$ relative to that heated at 120°C shows the presence of a group of pores which only permit limited capillary condensation. Some of the very wide pores seem to disappear with the appearance of others of smaller dimensions giving rise to mesopores with smaller average pore radius than those dried at 120°C. For the sample $(MC_3S)_3(950)$ a marked increase in pore size is noted changing the pore system from being predominantly microporous for the dried sample to completely mesoporous upon activation.

The hydration of these activated samples causes a decrease in specific area for the sample $(MC_3S)_1(950)$ whereas an increase is observed for the other two grain sizes. Since the initial hydration stage is usually characterized by an increase in specific area, as found for the samples $(MC_3S)_2(950)$ and $(MC_3S)_3(950)$, the hydrated

TABLE III

Surface characteristics of monoclinic and triclinic C_3S samples activated at 950°C and their corresponding hydrated samples

Sample	BET *C*-constant	S_{BET} m^2/g	S_t m^2/g	$V_{p(0.95)}$ ml/g	$\bar{r}_H$ nm
		Before hydration			
$(MC_3S)_1(950)$	3·0	73·8	65·0	0·1404	1·90
$(MC_3S)_2(950)$	2·0	62·0[a]		0·1201	
$(MC_3S)_3(950)$	4·0	64·0	60·0	0·1404	2·19
$(TC_3S)_1(950)$	3·5	59·6	55·0	0·1310	2·20
$(TC_3S)_2(950)$	3·0	67·8	62·0	0·1310	1·93
$(TC_3S)_3(950)$	3·0	61·7	59·0	0·1513	2·45
		After hydration			
$(MC_3S)_1(950)$	6·0	65·5	70·0	0·0871	1·33
$(MC_3S)_2(950)$	5·0	87·1	86·5	0·1154	1·38
$(MC_3S)_3(950)$	2·0	71·2[a]		0·0624	
$(TC_3S)_1(950)$	3·0	70·9	71·3	0·0858	1·21
$(TC_3S)_2(950)$	3·0	70·3	70·0	0·0757	1·08
$(TC_3S)_3(950)$	4·0	62·3	61·0	0·0677	1·09

[a] Areas obtained for the sake of comparison[29].

sample $(MC_3S)_1$ actually represents a more advanced hydration stage as also found from the analysis given before. The decrease in area observed for this second stage is attributed to the remarkable increase of the micro structure of the hydration products[5] whose pores are partly inaccessible to N_2. This is accompanied by a marked decrease in total pore volume resulting from the increase in the crystallite size of $Ca(OH)_2$ formed[30]. In all cases, the hydration is accompanied by a decrease in the average pore radius $\bar{r}_H$. This narrowing is clearly reproduced in the corresponding V_l–t plots of the activated samples before and after hydration (Fig. 8). Both samples $(MC_3S)_1$ and (MC_3S_2) show an upward deviation at a t-value of 0·50 nm that reverts back at a t-value of 1·00 nm with a larger increase in slope for the latter sample permitting more capillary condensation to occur. They contain both micro and meso pores, the latter being wider for the sample $(MC_3S)_2$.

The heating of triclinic C_3S samples decreased the specific area for the two smaller particle size samples, $(TC_3S)_1$ and $(TC_3S)_2$, whereas a small increase is observed for the sample $(TC_3S)_3$. Heating at 950°C was previously found to activate the surface and enhance its interaction with atmospheric water vapour. As these samples possess wide hysteresis loops it seems that some soldering of the particles has taken place, as such silicates usually form a sheet structure, the area decreases only slightly whereas the pore structure changes tremendously. The 8-mesh sample does not show this decrease in area.

This widening of the pore system is reflected in the V_l–t plots showing the predominance of mesoporosity. As initial upward deviation is observed that commences in the t-value range of approx. 0·56 nm with small decrease in slope at higher t-values but still remains above the straight line. This decrease in slope is

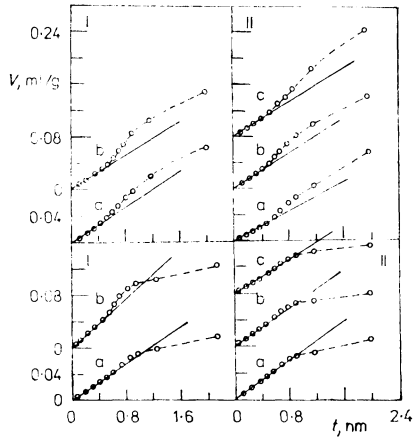

FIG. 8

V_l–t plots for monoclinic (I) and triclinic (II) C_3S samples activated at 950°C before and after hydration at 80°C for 60 days: a $(C_3S)_1$; b $(C_3S)_2$; c $(C_3S)_3$

marked for the sample $(TC_3S)_2(950)$, which, from the values of average pore radii, shows it to possess the smallest value. The widening of the pore system thus produced upon activation is evident and results from the agglomeration of the particles as in the monoclinic modification.

The hydration of activated triclinic C_3S causes an increase in specific area for all three grain sizes compared to the corresponding unhydrated samples. This increase in area is found to be accompanied by a corresponding decrease in both total pore volume. $V_{p(0.95)}$, and average pore radius $\bar{r}_H$ (Table III, columns 5 and 6). These variations appear as a result of the nature of the products formed. The water molecules adsorbed inside the pores give rise to the reaction products which mainly constitute tobermorite gel of higher area than the parent material[31]. These products possess lower density and larger volume[32], thus bringing about the observed narrowing in average pore radius and decrease in total pore volume. The increase in area of the sample $(TC_3S)_3$ is negligible inspite that the total pore volume and average pore radius are strongly affected. As this sample is least affected by hydration (previous section), the formed hydration products imposing the resulting textural variations seem to be still formed on the internal walls of the pores but are not yet extended into the solid matrix itself.

The drastic changes produced in the pore system upon hydration are reflected in the V_1–t plots (Fig. 8, II). In these plots most points fall on a straight line up to a t-value of 0·90 nm resulting from a compensation effect[33] between micro and meso pores. Above this t-value a downward deviation is observed confirming the presence of micro-pores. Thus much narrowing of the pore system has taken place upon, hydration reflecting the nature and texture of the newly formed hydration products.

REFERENCES

1. Chou P. I., Segalova E. E., Lukyanova O. I.: Kolloid Zh. *26*, 373 (1964).
2. Greenberg S. A., Chang T. N.: J. Phys. Chem. *69*, 553 (1965).
3. Fujii K., Kondo W.: *5th Int. Symp. Chemistry of Cement.* Tokyo 1968.
4. Stucks M. S., Majundar A. J.: Cem. Concr. Res. *7*, 711 (1977).
5. Harada T., Ohta M., Takagi S.: Yogo Kyokai Shi. *86*, 195 (1978).
6. Thomassin J. H., Regound M., Baillif P., Touray C. J.: C. R. Acad. Sci., C *288* (3), 93 (1979).
7. Ings B. J., Brown P. W., Frohnsdorff G.: Cem. Concr. Res. *13*, 843 (1983).
8. Fierens P., Trilocq J., Verhaegen J. P.: Cem. Concr. Res. *3*, 549 (1973).
9. Fierens P., Verhaegen J. P.: Cem. Concr. Res. *5*, 587 (1975).
10. Descamps J., Fierens P., Verhaegen J. P.: Gidratatsiya Tverd. Isem. *2*, 143 (1976).
11. Maycock J. N., Skalny J., Kalyoncu R.: Cem. Concr. Res. *4*, 835 (1974).
12. Hanafi S., El-Shafei G. M. S., Selim S. A.: Cemento *85*, 283 (1988).
13. Daimon M., Ueda S., Kondo R.: Cem. Concr. Res. *1*, 391 (1971).
14. Butt Yu. M., Timashev, V. V., Paramonova V. A.: Izv. Vyssh. Ucheb. Zaved., Khim. Khim. Tekhnol. *7*(3), 160 (1964).
15. Smith J. V. (Ed.): *X-Ray Powder Data File and Index to the X-Ray Data File*, ASTM, Philadelphia 1961.

16. *Powder Diffraction File, ASTM Alphabetical Index of Inorganic Compounds.* International Center for Diffraction Data, Philadelphia 1978.
17. Locher R. W.: Zem.-Kalk-Gips, *20*, 402 (1967).
18. Brunauer S., Greenberg S. A.: *Chemistry of Cement, Proceeding of the 4th Int. Symp.*, p. 135. Washington 1960.
19. Lippens B. C., Linsen B. G., de Boer J. H.: J. Catal. *3*, 323 (1964).
20. Mikhail R. Sh., Guindy N. M., Hanafi S.: Egypt. J. Chem. Special Issue "Tourky", *1973*, 53.
21. de Boer J. H.: *The Dynamical Character of Adsorption*, p. 34. Oxford University Press, London 1953.
22. Selim S. A., Philip Ch. A., Mikhail R. Sh.: Thermochim. Acta *39*, 267 (1980).
23. Dubinin M. M. in: *Characterizatin of Porous Solid, Proc. Int. Symp. 1978* (S. J. Gregg, K. S. W. Sing and H. F. Stoeckli, Eds), p. 1. Soc. Chem. Ind., London 1979.
24. Fierens P., Verhaegen J. P.: Cem. Concr. Res. *6*, 103 (1976); *6*, 287 (1976).
25. Jones P., Hockey J. A.: Trans. Faraday Soc. *67*, 2679 (1971).
26. Nakamoto K. (Ed.): *Infra Red Spectra of Inorganic and Coordination Compounds.* Wiley, New York 1978.
27. Taylor H. F. W. (Ed.): *The Chemistry of Cement*, Vol. 2, Appendix 1.
28. Buckle E. R., Gard J. A., Taylor H. F. W.: J. Chem. Soc. *1958*, 1351.
29. Gregg S. J., Sing K. S. W.: *Adsorption, Surface Area and Porosity*, p. 255. Academic Pres, New York 1982.
30. Diamon M., Abo-El-Enein S. A., Hosaka G., Goto S., Kondo R.: J. Am. Ceram. Soc. *60*, (3–4), 110 (1977).
31. Kantro D. L., Brunauer S., Weise C. H.: Adv. Chem. Series *33*, 199 (1962); J. Phys. Chem. *66*, 1804 (1962).
32. Skalny J., Young J. F.: *Mechanism of Portland Cement Hydration, Principle Report II-1, 7th Int. Congr. Chem. Cement*, Vol. 1. Paris 1980.
33. Mikhail R. Sh.: J. Chem. U.A.R. *6*(1), 27 (1963).